POWER DENSITY INFLUENCE ON LASER-INDUCED GRAPHITE STRUCTURAL MODIFICATIONS

L. AVOTINA[abc], A. MARCU[a*], M. LUNGU[a,c], A. STANCALIE[a], C.GRIGORESCU[d], A.G. ILIE[a], C. POROSNICU[a], L. MIHAI[a], D. SPOREA[a], C. LUNGU[a], S. SOMACESCU[e], G. KIZANE[b], D. SAVASTRU[d], S. ANTOHE[c,f]

[a]*National Institute for Laser, Plasma and Radiation Physics, 077125 Bucharest, Romania,*
[b]*Institute of Chemical Physics, University of Latvia, Jelgavas str.1, LV 1004 Riga, Latvia,*
[c]*University of Bucharest, Faculty of Physics, 405 Atomistilor Street, 077125, Magurele, Romania*
[d]*National Institute R&D for Optoelectronics INOE 2000, 077125 Bucharest, Romania*
[e]*"Ilie Murgulescu" Institute of Physical Chemistry, 202 Splaiul Independentei 060021, Bucharest, Romania,*
[f]*Academy of Romanian Scientists, Splaiul Independentei 54, 050094, Bucharest, Romania*

Graphite targets were irradiated with infrared (λ=800 nm) femtosecond (120 fs) and nanosecond (7 ns) laser pulses using comparable laser energy per pulse. Laser irradiation produced ablation and a superficial amorphisation of graphite in the centers of the irradiated zones whereas on their peripheries and in the depth of the target other structural modifications were observed. Micro-Raman investigations have shown a G-peak shift towards lower frequencies with the laser power density. That becomes particularly obvious for values in the range 10^7 - 10^9 W / cm^2 that also corresponds to a maximal increase of the sp^3 fraction. A maximum enlargement of the L_a - crystallite size at the surface of the target occurred for laser power density values ranging from 10^9 to 10^{11} W / cm^2. Beyond these limits both sp^3 fraction and L_a decrease suggesting a strong depreciation of the crystalline structure. XPS investigations have shown that sp^2 – sp^3 transition takes place below the ablation threshold and is also affected by the energy density value: a 1000 times variation in the power density produces comparable effects with a 10 times variation in the energy density. 'In-depth' XPS investigations have shown that sp^3 fraction increases as a cumulative process with the number of the laser pulses and confirms observed interdependence between injected power density and energy density.

(Received June 28, 2016; Accepted September 9, 2016)

1. Introduction

Carbon based materials including graphite, highly oriented pyrolytic graphite and carbon fiber composite (CFC) consisting mostly from polycrystalline graphite are used as divertor and limiter materials in fusion reactors [1,2]. In JET ITER like wall project (JET ILW) the divertor is mainly made of CFC covered with tungsten. Plasma-wall interaction induces changes in the structure of the plasma facing materials [3] leading to different behavior of the first wall and inducing potential plasma instabilities and seeding impurities. Further improvement of these materials relies on understanding the mechanisms of the occurring changes. At such high plasma energies injection speed is a crucial parameter involved in morphological and structural modifications of the exposed materials.

---

*Corresponding author: aurelian.marcu@inflpr.ro

Laser irradiation is one of the common approaches to replicate such high incident energies and power densities into the materials. For different wavelengths and pulse parameters various investigations were previously performed with several pulse energies and power densities. For example after irradiation of bulk graphite with 20-25 ns laser pulse of several tens of mJ energy the formation of disordered graphitic layer beneath ordered sp^2 hybridized nanocrystalline graphite [4] and phase explosion of the molten layer on the surface graphite [5] were observed. Femtosecond laser irradiations were mostly achieved with infrared laser pulses [6-15]. Carbon black formation was observed [6] after 100 fs (λ=800 nm) laser pulses with 0.1-0.7 J/cm^2 fluence while for a fluence of 90 J/cm^2 cubic diamond was obtained [7]. By exposing the samples to 50 fs pulses with the same wavelength, for fluencies of 0.2-2 J/cm^2 formation of nanocrystalline and amorphous carbon took place [8]. 800 nm, 120 fs laser pulses did show hexagonal diamond formation after 5.5 mJ/pulse irradiation [9] and carbyne and trans-polyethylene chains were produced after surface irradiation with 0.7 mJ/pulse [11]. Agglomeration of graphite nanoparticles was observed using λ = 1030 nm, 214 fs laser with power 15 W [12].

Power density is clearly one of the critical parameters for material structure induced modifications. In order to understand power density influences on the structural modifications taking place in the graphite under laser irradiation, some other influences (e.g. wavelength, pulse energy, etc.) have to be avoided. For this reason, in this study, the behavior of a graphite target was mainly investigated under the action of (single and multiple) femtosecond and nanosecond laser pulses operating at the same wavelength and having comparable spot sizes and energies per pulse.

2. Experimental system, techniques and approximations

Polycrystalline graphite samples were directly irradiated in air, at room temperature and wavelength λ = 800 nm with a femtosecond laser (120 fs, 6.7 mJ, [16]) and nanosecond laser pulses (Continuum FX-1 Sunlite Nd:YAG tunable laser, 7 ns, 10±1 mJ). The microstructure of the graphite target before and after irradiation was characterized by Scanning Electron Microscopy (SEM), using a 'FEI – INSPECT S' microscope, Raman spectroscopy (Horiba Scientific LABRAM HR800 Raman spectrometer, Ar^+ ion and HeNe laser sources operating at 488 and 633 nm, 100x objective, with 0.2 cm^{-1} resolution, integration time 30 s and Jasco Raman spectrometer with 633 nm and 532 nm, 100x objective, 1 cm^{-1} resolution, integration time 60 s, 3 accumulations). X-ray photoelectron spectroscopy (XPS) measurements were performed using Quantera SXM equipment, with a base pressure of 10^{-9} Torr in the analysis chamber. The X-ray source was Al K_α radiation (1486.6eV, monochromatized) and the overall energy resolution is estimated at 0.65 eV by the full width at half maximum (FWHM) of the $Au4f_{7/2}$ line. For the in-depth measurements, a standard etching of Ar ion sputtering beam with 2 keV (2x2mm) was used.
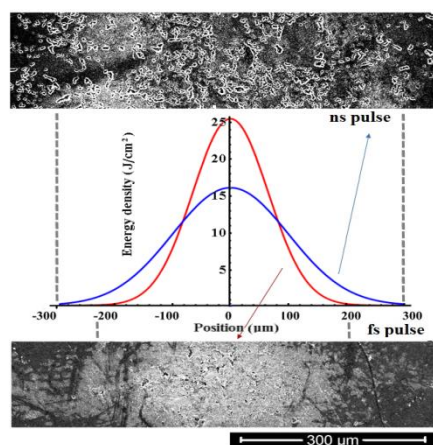

Fig.1. SEM images after ns and fs laser irradiation
and the power density spatial distribution functions

SEM images show the ablation in the middle of irradiated area after femtosecond and nanosecond exposure (Fig. 1). On the edges of irradiated areas non-homogeneous laser traces can

be observed. However, for both irradiation pulse duration the trace diameter is within 300 μm. The fluency distribution of the beams was approximated (2D) with Gaussian functions:

$$F_l = E_n \left(\frac{e^{-(x-\mu)^2/(2\sigma^2)}}{\sigma\sqrt{2\pi}} \right) \left(\frac{e^{-(y-\mu)^2/(2\sigma^2)}}{\sigma\sqrt{2\pi}} \right) \tag{1}$$

where F_l – laser fluence (J/cm^2); E_n – laser energy (J); x, y – positions (μm) from spot center μ – median ($\mu=0$ on both axis); σ – dispersion (approximated as equal on both axis).

The laser penetration depth into graphite target was calculated using the Beer-Lambert law and carbon absorption coefficient estimated by Hagemann [17]:

$$N_{photons}(z) = N_o e^{-\alpha z} \tag{2}$$

Thus, for λ=800nm the laser penetration depth was estimated to about 87 nm, while for the Raman laser sources the penetration depth values were ~40 nm for λ=488 nm, ~ 50 nm for λ=532 nm and ~70 nm for λ=633 nm.
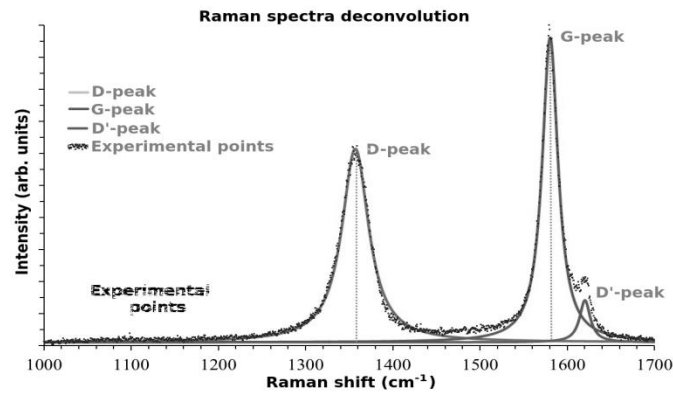

Fig.2. Example of a deconvolution of a Raman spectra for a femtosecond irradiated zone periphery area (with 3 peaks)

Raman spectra of the irradiated graphite targets (Fig. 2) shows a G-peak around 1580 cm^{-1} and two disorder related peaks, D (1330-1350 cm^{-1}) and D' (~1620 cm^{-1}). To extract the intensities and positions of the observed peaks we have performed the fit with Lorentz functions as shown in Fig.2 that stands for an example of a femtosecond irradiated zone periphery. The D-peak position ranges from 1330 to 1350 cm^{-1} (disperses with the used Raman excitation wavelength). The position of D'-peak is found around 1620 cm^{-1}. D and D' peaks appear in defected or disordered graphite [18].

The ratio between the intensities of D and G peaks (I_D/I_G - dotted lines in Fig.2.) is inversely proportional to the graphite crystallite size L_a [18, 19]. Thus, the expression further used for L_a crystallite size calculation is the one obtained by Cançado et all, respectively:

$$L_a(\text{nm}) = (2.4 \cdot 10^{-10}) \lambda_l^4 \left(\frac{I_D}{I_G} \right)^{-1} \tag{3}$$

where λ_l is the laser wavelength in nm, I_D/I_G in this case is the ratio of integrated intensities [20].
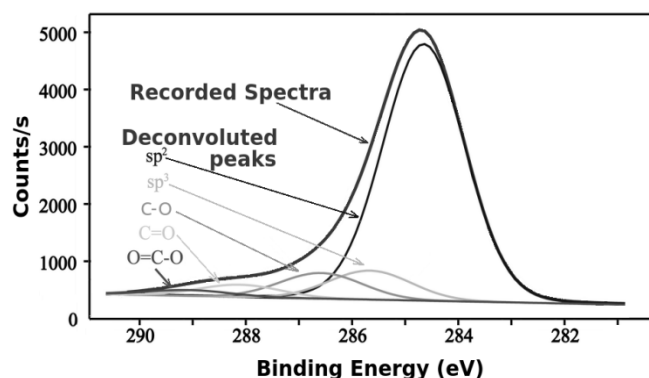
*Fig. 3 Example of a C1s photoelectron deconvoluted spectrum
(for a non-irradiated graphite zone)*

The Fig. 3 displays a representative XPS binding energy spectrum of the non-irradiated graphite target. We have extracted information on the existing carbon bonds after deconvolution of the raw XPS spectra. The spatial variation of the sp^3 fraction on the longitudinal spot axis is presented. To account for sp^3 'in-depth' variation the data corresponding to the non-irradiated area (attributed to Ar^+ bombardment during the measuring process) was subtracted from the curves obtained for the irradiated zones.

3. Experimental results and discussions

Raman measurements were performed for each of the fs and ns irradiated zones. By using the 488 nm laser source we obtained (Fig. 4a) information on the layers down to about 40 nm. For the ns irradiated area, the G-peak position shifts below 1580 cm^{-1} on the nanosecond irradiated spot peripheries, while in the center it moves up to about 1590 cm^{-1}. In the case of the femtosecond pulse the G-peak position shifts towards lower frequencies on the irradiation spot peripheries but an even more significant down shift can be observed in the center. By representing these variations as a function of the power density and fitting with polynomial functions the points corresponding to fluences below the ablation threshold a blue-shift tendency with increasing power density could be observed. Above 10^{10} W/cm^2 the trend became more evident. We noticed that for low power densities under the ablation plume the G-peak shifts towards higher frequencies corresponding to graphitization, possibly owing to the plume pressure and temperature effects [21]. On the contrary, for high power densities, even if ablation occurs but the ablation mechanism changes [22] and the heating effect is weaker [23] the G-peak shifts towards lower frequencies keeping the trend observed for the non-ablated area. Raman investigations with $\lambda = 633$ nm resulted in the G-peak shifts to lower values in the center of the irradiated zones for both nanosecond and femtosecond laser pulses. In the case of the femtosecond pulse irradiation the G-peak shift is not wavelength sensitive. Instead, for the nanosecond laser pulse irradiation in the central area there is no longer a shift to higher values but to lower values. This is clearly seen in the inset of Fig.4b.
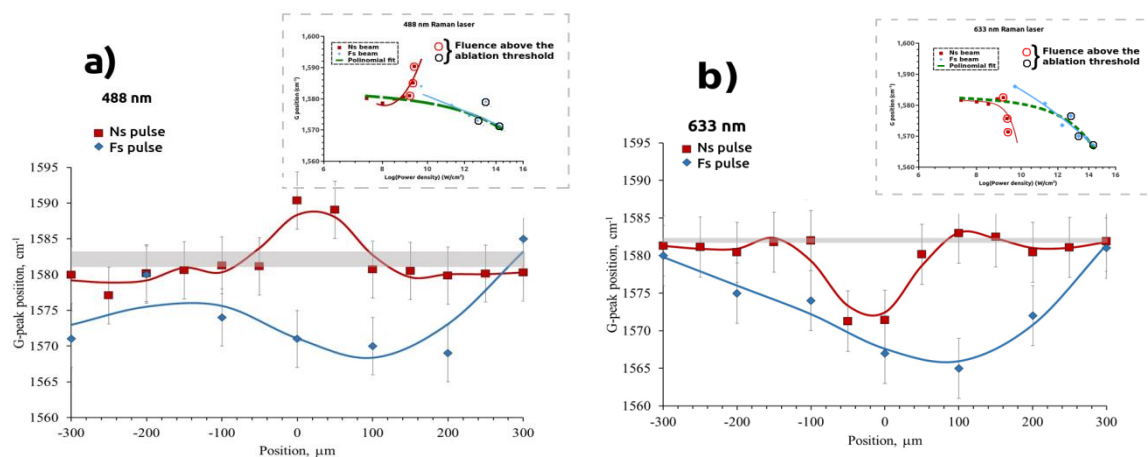
Fig. 4. Variation of the G-peak position after ns and fs laser beams irradiation,
investigated at a) 488 nm and b) 633 nm Raman laser wavelengths

The calculated crystallite size (L_a) from the 488 nm Raman data (Fig. 5a) on the fs irradiation area is close to the value found for the non-irradiated zone. We mention that graphite crystallite size in non-irradiated mirror polished graphite is in the range of 10-15 nm and it is represented by the gray line in the graphs. Using equation (2) we calculated L_a for the irradiated zone's points. The Raman ($\lambda = 532$ nm) mapping and computed L_a values for the ns-laser irradiated area are 3D plotted in Fig.5b to facilitate the overall visualization. About 300 micrometers away from the zone center the crystallite size slightly increases up to 17 nm. After ns irradiation, the crystallite size in the middle of the irradiated zones decreases below 10 nm while showing a slightly increasing tendency on the irradiated spot edges, similar to the fs laser case The variation of L_a with power density (for fluences below the ablation threshold) is displayed in the Fig. 5a inset. One can notice a slightly increasing trend of L_a up to power densities of 10^{-9} – 10^{-11} W/cm^2 and a slight decrease for power density values above 10^{11} W/cm^2. The points corresponding to fluences above the ablation threshold suggest a stronger shrink of L_a. If for the higher power densities it might be questionable whether the fs-laser ablation would influence at all on the L_a decrease, when looking at the lower power densities (i.e. the ablation points corresponding to the ns-pulse) the plume influence in reducing the L_a value at the target surface became indubitable. Like in the G-peak shift case discussed at the beginning of this section, we attempt to attribute the differences to the higher temperature and pressure in the ns-ablation and possibly to oxidations and other plume related processes.

When calculating L_a for $\lambda=633$ nm we remarked that for deeper layers (down to about 70 nm) its value is significantly larger in the irradiation zone for both ns~ and fs-laser spots. After irradiation with one ns-laser pulse L_a increases to about 27 nm while keeping the surface trend (i.e. like for $\lambda = 488$ nm), and slightly decreases in the center, where ablation takes place (Fig. 5b). However, L_a decrease is significant below the spot center. After fs laser irradiation the crystallite size has only a slight decreasing tendency in the center. In terms of power density, for layers down to 70 nm L_a tends to rather increase with increasing power density up to 10^7 - 10^8 W/cm^2 but without significant variations beyond that limit. There is weak decrease tendency in the 10^{13} – 10^{14} W/cm^2 interval (corresponding to the 'weak' plume in the fs laser irradiation). And a strong decrease around 10^9 mW/cm^2 (corresponding to the stronger plume in the ns regime) By summarizing the two L_a investigations, there seems to be a L_a maximum for within 10^9 – 10^{10} W/cm^2 range at the surface (down to about 40 nm) and a within 10^{10} – 10^{11} W/cm^2 range for deeper layers (down to about 70 nm) while plume presence decreases this value through some associated processes.
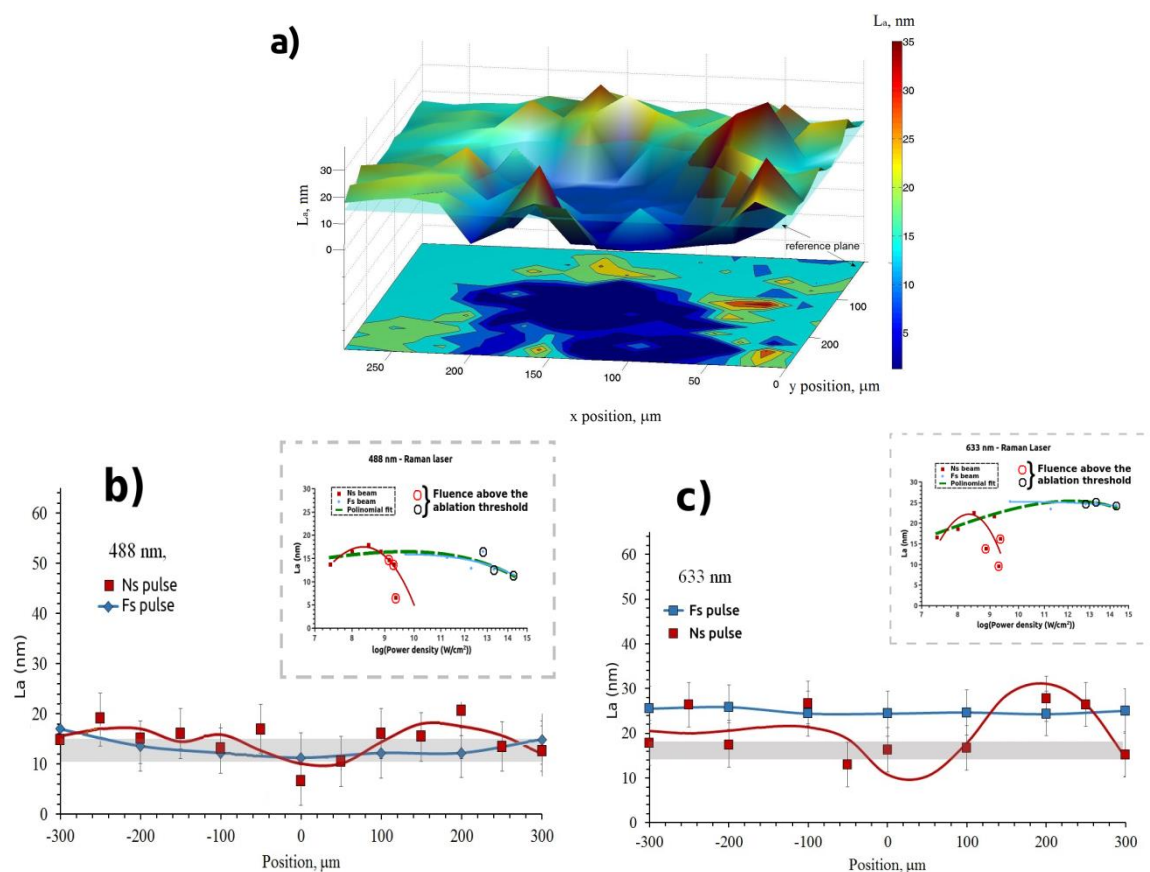
Fig. 5. L_a calculations for a) nanosecond beam irradiation investigated with 532 nm and a comparison of ns and fs laser irradiation investigated with b) 488 nm and c) 633 nm Raman laser wavelengths

From XPS spectra the variation of sp^3 fraction was extracted up to a few nm depth from the surface. An increase of the sp^3 fraction on the spot peripheries was observed in the case of the ns laser beam while a decrease was obtained for the fs pulse irradiated zone. An increase of sp^3 fraction in the center of a fs beam was obtained only for a very low fs pulse energy (0.65 mJ). For higher fluences of the fs beams a decrease of the sp^3 fraction is remarked, which seems to correspond to an amorphization process at the target surface. The variation of the sp^3 fraction with the laser fluence (Fig. 6a) shows a slightly increasing tendency only for fluence values around the ablation threshold. For high fluence (and respectively higher pulse energies) there is a clear decrease of the sp^3 fraction particularly in the plume forming spots. The sp^3 fraction as a function of laser power density touches its maximum within 10^8 - 10^9 W/cm². The pulse energy and the fluence also affect significantly the sp^3 fraction values. It appears from our results {Fig. 6c) that increasing the power density by 4.5 orders of magnitude and decreasing by 1.5 orders the pulse energy density yields in identical sp^3 fraction values. Furthermore, by selecting on the curves spots with comparable fluence but corresponding to different pulse energies, we could derive the effects of power density versus fluence and energy over sp^3 fraction. Tracing for example the 2 and 5 J/cm² points on the presented cases, one can see that for comparable power densities (around 10^{13} – 10^{14} W/cm²s) the increase of the injected energy could lead to a local increase or decrease of sp^3 fraction depending on the total pulse energy. For the 0.65 mJ where the ablation plume is practically not forming the sp^3 percent is increasing (as in the 'ablation plume vicinity' cases). With the increase of the pulse energy, when formation of the ablation plume starts, the sp^3 fraction value stops increasing and even starts decreasing. Thus, even for the fs beam case, (where is considered a low heat propagation into the target material [23]) there are some plume-associated direct and indirect processes that affect the neighborhood zones owing to the pulse total energy. Summarizing the results, there is a certain increase of the sp^3 fraction for power densities up to about 10^9 W/cm², but there is also a certain correlation between the energy amount injected and the injection speed

for achieving a maximum sp^3 fraction increase. A 10^3 times increase in the power density is likely to have a similar effect with a 10 times increase in the injected energy density. The plume formation leads to a decrease of the sp^3 fraction on the target surface.
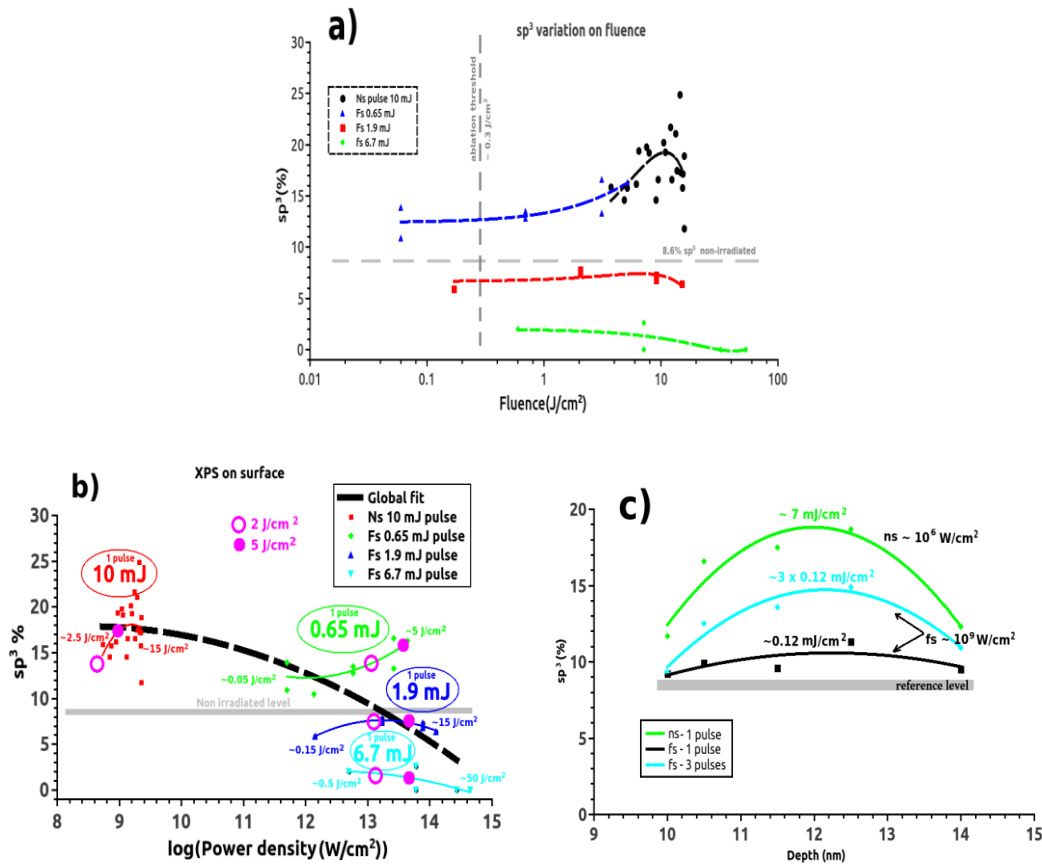

Fig. 6 sp^3 fraction estimations on the target surface a) as a function of laser fluence, b) as a function of power density and c) 'in-depth' estimated variation.

With further 'in-depth' investigations made below the irradiation zones (but outside the plume forming areas) we could remark similar trends for the fs and ns beams. The sp^3 fraction increases with a maximal value around 12 nm in the investigation points from both, ns and fs beams (Fig. 6b) and for one and three laser pulses. The difference in the variation curves is only the peak amplitude. These results mainly suggest that the sp^3 fraction is a cumulative process, the effects increasing with the number of pulses as previously reported [13]. Considering the effect of power density on the sp^3 fraction it is to remark that a 10 % increase could be obtained with a 10^6 W/cm^2 and about 7mJ/cm^2 while a 2% increase would with 10^9 W/cm^2 but with only 0.12 J/cm^2. With 3 pulses of 0.12 mJ/cm^2 at 10^9 W/cm^2, we obtain a 5 % sp^3 fraction increase, respectively half of the ns pulse effect. Thus, by considering the injected energy for a 1% increase of the sp^3 fraction we could conclude again that a 3 order increase of the power density led to decreasing by one order of magnitude the amount of the energy density for a comparable effect. However, since these measurements were performed on the periphery of the irradiated zones, the 'in-depth' measurements conclusions could be considered true in the absence of the ablation plume.

4. Conclusions

A polycrystalline graphite target was irradiated with ns (7 ns) and fs (120 fs) IR (λ=800 nm) laser pulses with comparable energies (~ 10 mJ and respectively ~ 6.7 mJ) and spot size, in

order to investigate power density influences on the laser induced modifications of the graphite structure. Micro-Raman investigations have shown a down-shift of the graphite G-peak position with the increase of the power density, more evident for power densities above $10^7 - 10^9$ W/cm^2. The range also corresponds to an enhancement of the sp^2 - sp^3 transitions shown by the XPS surface measurements. The 10^9-10^{11} W/cm^2 interval corresponds to a maximum L_a – crystallite size. Beyond these power densities G-peak keeps shifting to lower frequencies, the crystallite size decreases while sp^3 fraction starts decreasing too, suggesting a stronger depreciation of the target crystalline structure. The tendencies are more evident at some tens of nanometers below the surface. Formation of an ablation plume could further contribute to accelerating the G-peak shift and the decrease of the L_a, independent of the power density regime. XPS investigations have shown that sp^2 – sp^3 transition is a cumulative processes with the total injected energy, but it is also controlled by the power density, supporting the hypothesis of its indirect photonic source. Thus, a higher power laser density could be more efficient for inducing sp^2-sp^3 transitions, e.g. three orders of magnitude in power density variation produce comparable results with one order variation in the energy density.

References

[1] S. Nakamura, S. Sakura, H. Ozaki, Y. Seki, K. Yokoyama, A. Sakasai, D. Tsuru, Fus. Eng. Des. **89,** 1004 (2014).

[2] Y. Corre, R. Dejarnac, J.-L. Gardarein, J. Gaspar, F. Escourbiac, E. Gauthier, J.P. Gunn, M. Komm, M. Lipa, T. Loarer., M. Missirlian, F. Rigollet, article in press (2014), http//dx.doi.org/10.1016/j.nucmat.2014.10.036

[3] T.D. Burchell, J.P. Strizak, Nuc. Eng. Des. **271,** 262 (2014)

[4] M. Bonelli, A. Miotello, P.M. Ossi, A. Pessi, S. Gialanella, Phys. Rev. B **5**, 13513 (1999)

[5] S.I. Kudryashov, A.A. Tikhov, V.D. Zvorykin, Appl.Phys A **102**, 493 (2011)

[6] S.I. Kudryashov, J. Appl. Phys. **100**, 036103 (2006)

[7] R. Nüske, A. Jurgilaitis, H. Enquist, M. Harb, Y. Fang, U. Håkanson, J. Larsson, Appl. Phys. Lett. **100**, 043102 (2012)

[8] P. Feng, N. Zhang, H. Wu, X. Zhu, Opt. Lett. **40**, 17 (2015)

[9] T. Sano, K. Takahashi, A. Hirose, O. Sakata, M. Okoshi, N. Inoue, K.F. Kobayashi, Mat. Sci. For. **561-565,** 2349 (2007)

[10] A. Marcu, L. Avotina, A. Marin, C.P. Lungu, C.E.A. Grigorescu, N. Demitri, D. Ursescu, C. Porosnicu, P .Osiceanu, G. Kizane and C. Grigoriu, J. Phys. D: Appl. Phys. **47**, 355305 994 (2014)

[11] A. Hu, M. Rybachuk, Q.-B. Lu, W.W. Duley, Appl. Phys. Lett. **91**, 131906 (2007)

[12] M. Sivakumar, B. Tan, K. Venkatakrishan, Appl. Surf. Sci. **257**, 9780 (2011)

[13] A.Marcu, L.Avotina, C.Porosnicu, A.Marin, C.E.A.Grigorescu, D.Ursescu, M.Lungu, N.Demitri and C.P. Lungu" App. Surf. Sci. **335**, 477 (2015)

[14] L. Avotina, A. Marcu, C. Porosnicu, M. Lungu, A. Stancalie, A.G. Ilie, P. C.Ganea, D. Savastru, J. Kalnacs, C.P. Lungu, G. Kizane, S. Antohe", Dig. J. Nanomat. Biostr. **11,** 293 (2016).

[15] M. Lungu, I. Tiseanu, C. Porosnicu, C. Dobrea, I. Jepu, P. Dinca, A. Marcu, C. P. Lungu, Dig. J. Nanomat. Biostr., **11,** 401 (2016).

[16] R. Dabu, R. Banichi, B. Blanaru, C. Fenic, L. Ionel, F. Jipa, L. Rusen, S. Simion, A. Stratan, M. Ulmeanu, D. Ursescu, M. Zamfirescu, J. Optoelectron. Adv. M. **12**, 35 (2010)

[17] H.-J. Hagemann, W. Gudat, C. Kunz, J. Opt. Soc. Am., **65**, 742 (1975)

[18] J. Schwan, S. Ulrich, V. Batori, H. Ehrhardt, S.R.P. Silva, J. Appl. Phys. **80**, 440 (1996)

[19] S.D. Knight, W.B. White, J. Mater. Res. **4**, 385 (1989)

[20] L.G. Cancado, K. Takai, T. Enoki, M. Endo, Y.A. Kim, H. Mizusaki, A. Jorio, L.N. Coelho, R. Magalhaes-Paniago, M.A. Pimenta, Appl. Phys. Lett. **88**, 163106 (2006)

[21] Q. Nian, Y. Wang, Y. Yang, J. Li, M. Y. Zhang, J. Shao, L. Tang and G. J. Cheng, Sci. Rep. **4** 6612 (2014)

[22] M.Stafe. A. Marcu and N. Puscas, "Pulsed Laser Ablation of Solids (Basic, Theory and Applications)", Springer, Heidelberg (2014)

[23] W. Kautek, S. Mitterer, J. Kr¨uger, W. Husinsky and G. Grabner, Appl. Phys. A **58**, 513 (1994).